National Conference with International Participation
ENGINEERING MECHANICS 2006
Svratka, Czech Republic, May 15 – 18, 2006
paper no. 196

PREDICTION OF THERMALLY INDUCED PRELOAD IN HIGH-SPEED BEARING SYSTEMS

T. Holkup[1], S. Holý[2]

Summary: *Increased use of high-speed machining creates the need to predict spindle behaviour at high speeds. Particularly, prediction of bearing failures caused by excessive thermally induced preload is one of key issues in the design of high-speed machine tool spindles. There is a need for optimization of spindle bearing system and of its surroundings, which could be enabled by a coupled thermo-mechanical model. However such a model must consider all physical fields involved in the problem.*

1. Introduction

Most problems of modern high-speed spindles are caused by heat generated within the spindle and by the mechanical consequences of the structure's warming. A heat flow model is presented in (Bossmanns & Tu, 1999) and it accounts for all major heat sources within the spindle system, such as:

- heat generation by angular contact ball bearings under the influence of speed and preload
- heat generation by the electric motor in rotor and stator as a function of torque and speed.

Preloaded angular contact ball bearings (ACBBs) are commonly used to obtain high stiffness of machine tool spindles. However, a potential thermal instability due to positive feedback in the 'preload-heat' closed loop is a serious drawback, as shown in Fig.1.

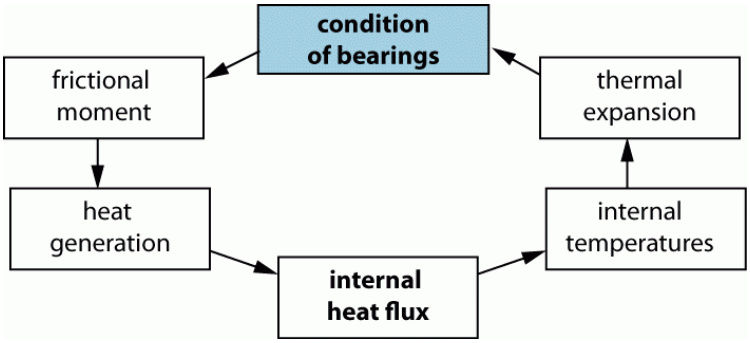

Fig. 1: 'Closed-loop' mechanism of thermally induced preload

[1] Ing. Tomáš Holkup: Research Centre of Manufacturing Technology, Faculty of Mechnical Engineering, Czech Technical University in Prague; Horská 3; 128 00 Praha 2; tel. +420 605 205 936; e-mail: t.holkup@rcmt.cvut.cz
[2] Prof. Ing. Stanislav Holý: Division of Strength of Materials, Faculty of Mechnical Engineering, Czech Technical University in Prague; Technická 4;166 07 Praha 6; e-mail: stanislav.holy@fs.cvut.cz

According to this closed loop mechanism, heat produced by bearings causes thermal growth and thermal expansion of the spindle parts and may cause the contact force (preload) to increase. The preload force further increases the bearing friction heat generation, and as a result the bearing may become overloaded, and even seizure can occur. This is noted as the thermally induced preload problem (Bossmanns & Tu, 1999), (Spiewak & Nickel, 2000) or (Stein & Tu, 1994).

2. Scheme of proposed model

A general preload model cannot be created by a standard finite element method (FEM) approach, because some of thermal and structural properties of bearings (e.g. heat generation, contact conduction, bearing rigidity) are coupled and dependent on the instantaneous thermo-mechanical condition of the spindle. For the purpose of updating these parameters, the transient problem is solved in discrete time-steps, Fig. 2, and after each step new bearing properties are calculated. If the time step is small enough, the solution flow should represent the real coupled transient behaviour. It is necessary to determine following in each step:

- thermal field, with known thermal input data can be solved by FEM
- deformations, with known thermal field and load can be solved by FEM
- internal condition of bearings, determined by system of algebraic equations

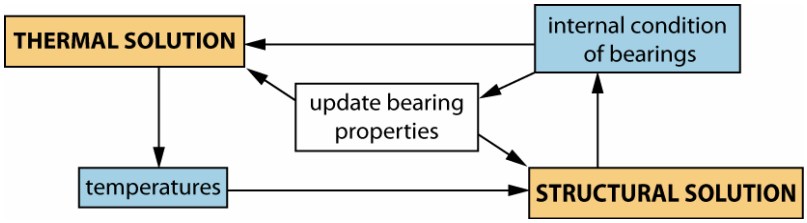

Fig. 2: Solution flow diagram

Such a structure of the analysis was performed in ANSYS FEM software using its APDL programmer's environment. ANSYS offers the possibility to build several 'physical environments' on one model. This feature and the overall openness of ANSYS for user-programmed routines were employed to build the coupled model.

The bearings are not modelled 'in detail', but as simplified objects, whose properties are functions of preload, speed, etc. Nevertheless validity of this approach is conditioned by exact knowledge of these functions. To make this model valid, it is necessary to know following functions for updating the analysis. Indexes *o* and *i* refer to outer and inner raceway contact respectively:

- contact stiffness coefficients k_o , k_i from (1)
- heat flow generated in bearing P_o, P_i proportional to contact forces and speed
- thermal resistances of the ball-ring contacts R_o , R_i proportional to contact forces
- thermal resistances of the shaft-bearing and housing-bearing contacts

Some of these can be figured out using available literature: bearing catalogues, (Bossmanns & Tu, 1999), (Harris, 1971), (Nakajima, 1995), some are just guessed yet and will be determined with a help of experiments. The character of the problem shows, that mainly accuracy of the heat production characteristic plays the key role.

3. Bearing model

The bearing model solves the 'internal condition' of bearings (contact forces, angles, rigidity) as the result of the 'external condition' calculated by FEM analyses.

The assumption of fully axisymmetrical behaviour will be used in following text and the force and stiffness coefficient values are valid for the whole bearing (summation for all balls).

In high speed operation of ball or roller bearings the rolling element centrifugal forces can be significantly large compared to the forces applied to the bearing externally. High speed affects the contact forces and angles, Fig. 3, and also the dynamics of the bearing-supported rotor system.

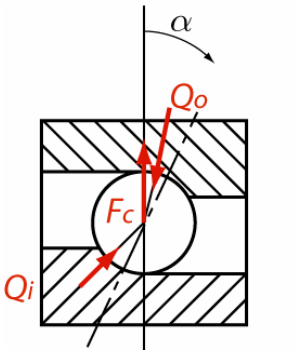

Fig. 3: Ball loading

In (Harris, 1971) were derived formulas for determination of bearing internal condition. Input data are:

- **constant**, bearing geometry, material, stiffness of contacts; usually could be obtained from bearing manufacturer
- **variable**, determining the 'external condition' of the bearing; according to type of preload the input data are: raceways curvature centres relative displacement (d_a axial and d_r radial), speed n and axial force F_a on outer ring respectively, see Tab. 1.

Basic formulas rise from the Hertzian theory. For normal loads Q and normal deformations d can be written for both contacts:

$$\begin{aligned} Q_o &= k_o d_o^{\frac{3}{2}} \\ Q_i &= k_i d_i^{\frac{3}{2}} \end{aligned} \tag{1}$$

Gyroscopic moments are neglected in further solution, like in (Li & Shin, 2004), and according to Fig.3, for equilibrium of forces in axial and radial directions can be written:

$$\begin{aligned} Q_i \sin\alpha_i - Q_o \sin\alpha_o &= 0 \\ Q_i \cos\alpha_i - Q_o \cos\alpha_o + F_c &= 0 \end{aligned} \tag{2}$$

where α_o, α_i are the contact angles and F_c the total centrifugal force on the mass of all balls.

$$F_c = \omega_b^2 m_b \frac{D_m}{2} \doteq \left(\omega \frac{D_i}{(D_o + D_i)}\right)^2 Z \rho_b \frac{4}{3}\pi \left(\frac{D_b}{2}\right)^3 \frac{D_m}{2} \tag{3}$$

where D_b and D_m are the ball and the mean bearing diameter; D_o and D_i are the outer and inner raceway diameter; Z number of balls and ρ_b is the ball material density.

Under zero load the centres of the raceway groove curvature radii are separated by a distance *BD* defined

$$BD = \left(f_o + f_i - 1\right) D_b \tag{4}$$

as shown in Fig.4, where the contact geometry is described by non-dimensional parameters

$$f_o = \frac{r_o}{D_b} \qquad f_i = \frac{r_i}{D_b} \tag{5}$$

where r_o, r_i are the ring curvature radii in plane normal to race tangent.

In accordance with relative axial and radial displacement of the ring curvature radii centres, with α as the initial contact angle, the distances in both directions are

$$A_1 = BD \sin\alpha + d_a \qquad A_2 = BD \cos\alpha + d_r \tag{6}$$

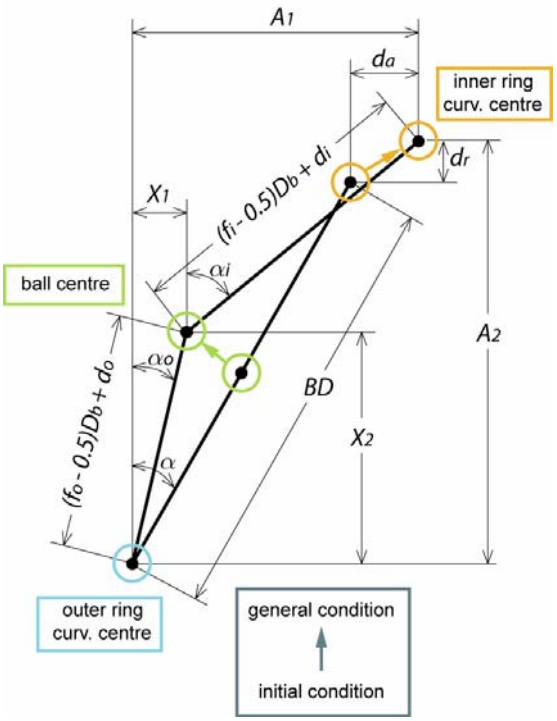

Fig. 4: Ball position diagram

After substitution of previous formulas into (2) and into geometrical functions derived from Fig. 4 we obtain four equations stating the relationship between the 'external' and 'internal' condition of an ACBB.

$$\left(A_1 - X_1\right)^2 + \left(A_2 - X_2\right)^2 - \left[\left(f_i - 0.5\right) D_b + d_i\right]^2 = 0 \tag{7}$$

$$X_1^{\,2} + X_2^{\,2} - \left[\left(f_o - 0.5\right) D_b + d_o\right]^2 = 0 \tag{8}$$

$$\frac{K_i d_i^{\frac{3}{2}} \left(A_1 - X_1\right)}{\left(f_i - 0.5\right) D_b + d_i} - \frac{K_o d_o^{\frac{3}{2}} X_1}{\left(f_o - 0.5\right) D_b + d_o} = 0 \tag{9}$$

$$\frac{K_i d_i^{\frac{3}{2}} \left(A_2 - X_2\right)}{\left(f_i - 0.5\right) D_b + d_i} - \frac{K_o d_o^{\frac{3}{2}} X_2}{\left(f_o - 0.5\right) D_b + d_o} + F_c = 0 \tag{10}$$

When constant preload of ACBB is used, equation $F_a = Q_o \sin\alpha_o$ with an appropriate substitution must be added. The most probable method of simultaneous iterative solution of these nonlinear equations is the Newton-Raphson method:

$$\mathbf{X}_{i+1} = \mathbf{X}_i - [J(\mathbf{X}_i)]^{-1}\, \mathbf{F}(\mathbf{X}_i) \tag{11}$$

where **X** is the vector of unknowns and $J(\mathbf{X}_i)$ is the Jacobian matrix of equation vector **F** with substituted **X** values from last iteration. The solver was programmed in MATLAB using the Symbolic Math Toolbox.

In further solution two main types of bearing application must be distinguished, position and constant preload, Fig. 5 and Fig. 6. This determines what is given to the bearing by mating parts and how the internal equilibrium occurs. Summary is given in Tab. 1. Results are also ball spin and roll velocities relative to the shaft speed and the frictional moment due to ball spin proportional to contact ellipse geometry, as described in (Harris, 1971).

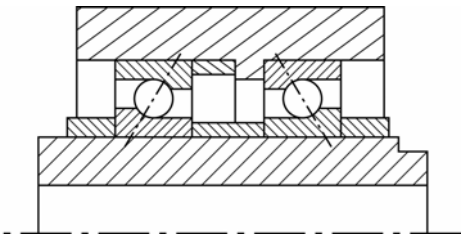

Fig. 5: Position preload

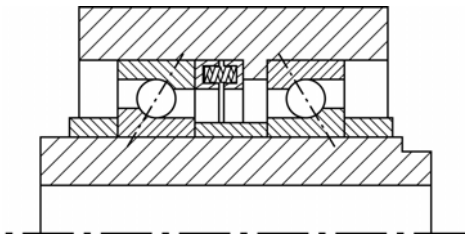

Fig. 6: Constant preload

Bearing rigidity is obtained by additional calculations with slightly varied input displacements. By observing the change in contact forces the stiffness in both directions can be determined.

Tab. 1: Bearing model summary

	Position preload	***Constant preload***
input data - constant	D_b , D_m , r_o , r_i , ρ_b , α, k_o , k_i	
input data - variable	d_a , d_r , n	d_r , n , F_a
number of equations	*4*	*5*
primary results	Q_o , Q_i , α_o , α_i	Q_o , Q_i , α_o , α_i , d_a
secondary results	K_a , K_r	K_r
other results	ω_{roll}/n , ω_{spin}/n , $M_{f\ spin}$	

Position preload of bearings

There are examples of calculations on SKF 7010 CD all-steel bearing in following figures. Contact forces, angles and rigidity are displayed as a function of speed. For a general comparison, characteristics of a virtual hybrid bearing (with ceramic balls) are added. This bearing is assumed of the same contact stiffness showing just the effect of centrifugal forces.

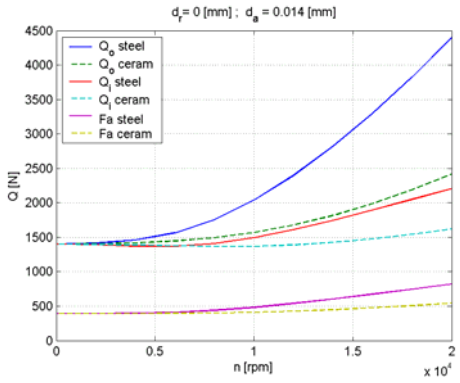

Fig. 7: Contact forces, preload vs. speed

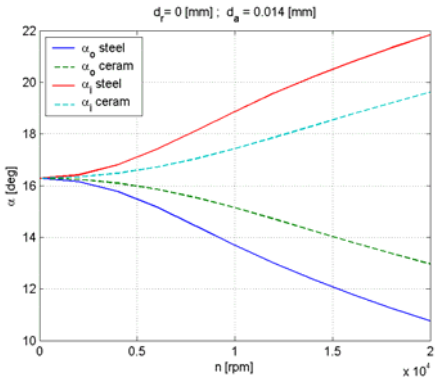

Fig. 8: Contact angles vs. speed

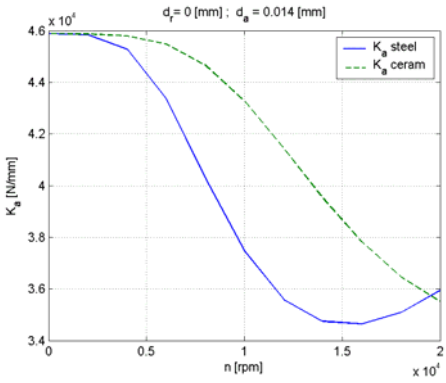

Fig. 9: Axial stiffness vs. speed

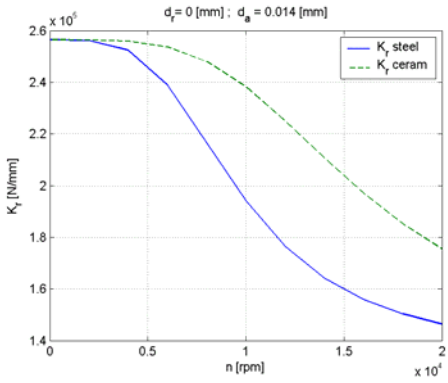

Fig. 10: Radial stiffness vs. speed

In Fig. 11, Fig. 12 respectively contact angles for various d_a , d_r at a particular speed are shown. The downthrow in Fig. 11 is an indication of a d_a , d_r combination that has no real solution: the bearing is either unloaded or reverse oriented.

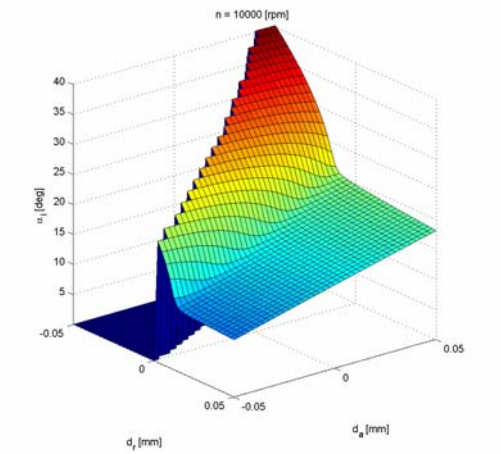

Fig. 11: Inner contact angle at 10 000 rpm

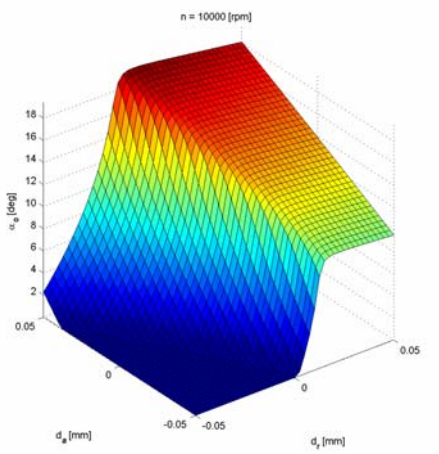

Fig. 12: Outer contact angle at 10 000 rpm

Constant preload of bearings

Similar calculations were carried out for the same, spring preloaded, bearing. Contact forces and angles were observed at a particular speed as a function of spring thrust load.

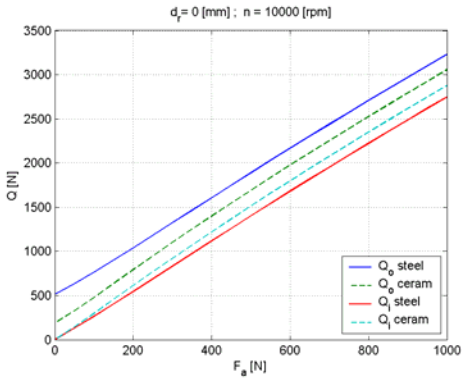

Fig. 13: Contact forces vs. thrust load

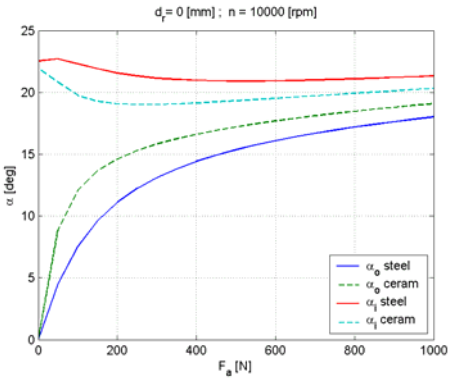

Fig. 14: Contact angles vs. thrust load

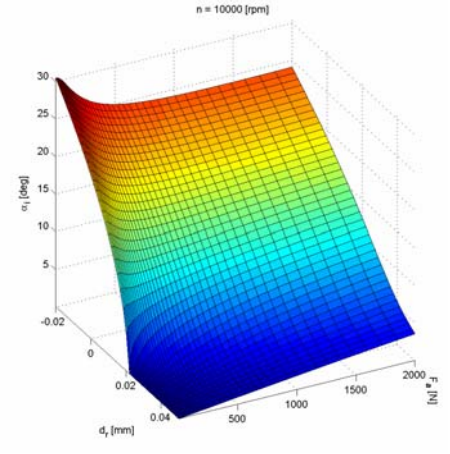

Fig. 15: Inner contact angle at 10 000 rpm

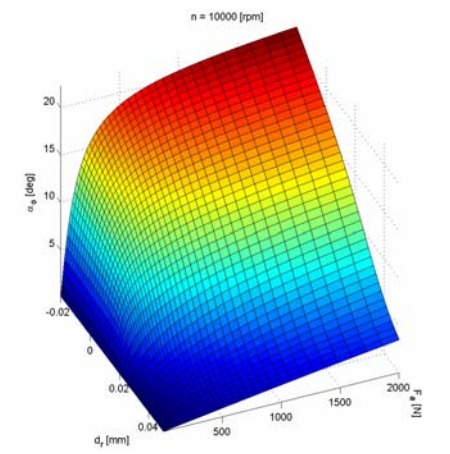

Fig. 16: Outer contact angle at 10 000 rpm

4. Coupling the bearing model with FEM

In order to couple the bearing model with advantages of FEM we cannot employ only one software without programming the FEM by ourselves as done in (Bosmanns & Tu, 1999) or (Li & Shin, 2004).

Different way presented here is to determine the 'external condition' parameters, to prescribe their expected intervals and to calculate all their combinations sufficiently fine. Such an output data can be arranged into multidimensional arrays, one array for each result parameter from Tab. 1. Arranged arrays can be read by the FEM software (ANSYS) and used as tabular data for interpolation.

Both position and constant preload applications are described by combination of three variables and 3D arrays are generated as shown in Fig.17. Examples of layers from these arrays are displayed in Fig. 11, Fig. 12, Fig. 15 and Fig. 16.

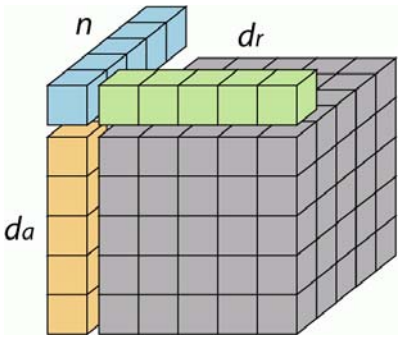

Fig. 17: 3D array for position preload

Moving bearing nonlinearities out from FEM has several advantages together with the axisymmetric concept of the model: no convergence difficulties, short time of solution, easy debugging of the solution process and comfortable tracing of any parameter.

5. Thermal solution

The task of thermal solution is to determine temperatures for following structural solution. The data flow is displayed in Fig. 18. The following assumptions are made:

- at each ball-ring contact half of the generated heat enters the ring and half enters the ball
- each raceway curvature is of uniform temperature to smooth the heat impact in FEM
- contact thermal resistances between bearing rings and spindle parts (housing, shaft) are neglected

A simplified thermal model of a grease-lubricated bearing is displayed in Fig.19. P_o and P_i represent heat flow generated on a particular contact; R_o and R_i the ball-ring contact resistances; C_b is the thermal capacity of all balls.

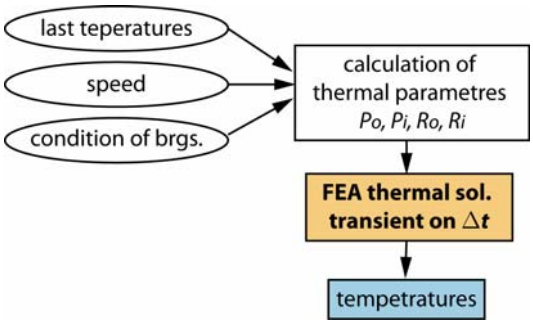

Fig. 18: Data flow during thermal solution

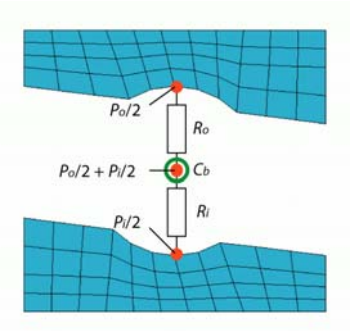

Fig. 19: Bearing thermal model

The generated heat is assumed to be a sum of the load-, viscous- and spin-depended contributions (Harris, 1971), (Li & Shin, 2004).

$$P = M_{f\_load}\omega_{roll} + M_{f\_visc}\omega_{roll} + M_{f\_spin}\omega_{spin} \tag{12}$$

Nevertheless the pure theoretical estimation of frictional moments was not in a good agreement with results obtained by 'coast tests' performed on our test spindle. During a 'coast test' (Bossmanns & Tu, 2001) the spindle is quickly started and after immediate disconnection slows down to a standstill. The friction torque (function of speed and bearing preload) calculated from the spindle angular deceleration is proportional to the heat generation in bearings. In order to fit our experimental results, correction coefficients were added into theoretical formulas.

A general unsymmetrical triplex bearing set has been modelled to represent a simplified spindle system, as shown in Fig. 20. Convection of ambient air as the only heat sink was introduced on appropriate surfaces together with heat transfer through the air cavity between rotating and stationary spindle parts. The FEM thermal analysis runs on a defined time interval and is restarted after the structural solution updates internal condition of bearings.

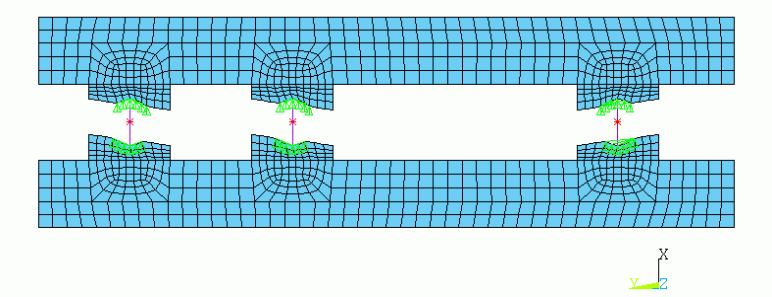

Fig. 20: Bearing assembly, thermal physical environment

6. Structural solution

The structural model solves deformations (external bearing condition) together with sequential update of bearing internal condition, as depicted in Fig. 21.

Rolling elements are ignored in structural FEM and appropriate forces are introduced on the races instead.

In postprocessor of the structural solution the relative displacement of bearing rings is read. Together with the information of the ball thermal expansion and the bearing initial fit it is taken into consideration for stating the resultant external bearing condition d_a , d_r for each bearing separately.

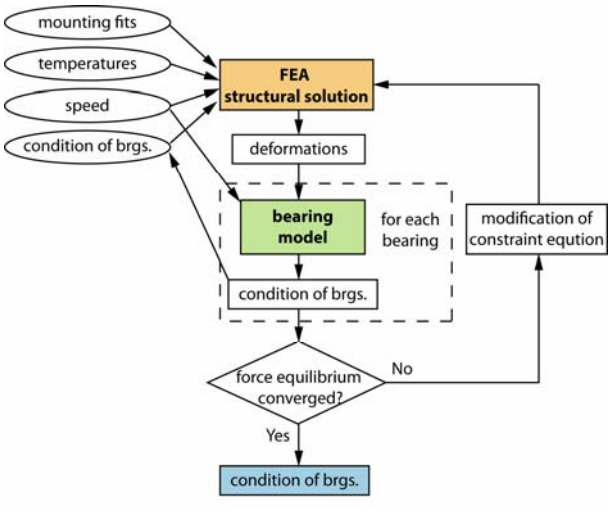

Fig. 21: Data flow during structural solution

If the bearing set is unsymmetrical, relative shaft-housing displacement due to unbalanced axial forces in bearings must be expected. An internal cycle is programmed to accommodate the displacement by modification of a constraint equation connecting the housing-shaft relative axial displacement. The Newton-Raphson logic is used for finding the force equilibrium with known force unbalance F_{a_mov} and the total axial stiffness of the spindle K_{a_tot} (actually the derivation of F_{a_mov}) by a convergence shaft shift d_{a_mov} according to (13) in each convergence cycle. The solution converges without difficulties in several equilibrium iterations. The process is modified appropriately for position and constant preload.

$$d_{a\ mov} = \frac{F_{a\ mov}}{K_{a\ tot}} \tag{13}$$

7. Simulation

To perform the above-described analysis in ANSYS, a parametric program in APDL language was developed. The modelled spindle is depicted in Fig. 29 together with its FE representation in Fig. 20. Thermal and structural analyses turn according to Fig. 2, and bearing condition is updated according to the instantaneous thermo-mechanical state.

By modifications of the speed parameter, the thermo-mechanical behaviour of the system changes, preload in time for various speeds is displayed in Fig. 22. The term ‘preload’ mentioned here is understood as the axial member of the contact force acting on the outer ring of the single bearing 1 (numbered from right in Fig. 20). Similarly the temperatures plotted in Fig. 23 are the temperatures of the outer race contact of the single bearing 1. The right bearing is chosen because its preload is a sum of unevenly distributed load between two left bearings, the distribution is shown in Fig 24.

It is obvious that when further increasing the speed, the model becomes unstable and preload and temperatures will rise quickly without bound. This means seizure of the spindle in practice. Similar behaviour of the model is observed also when changing the initial preload or convection heat sinks on spindle surfaces.

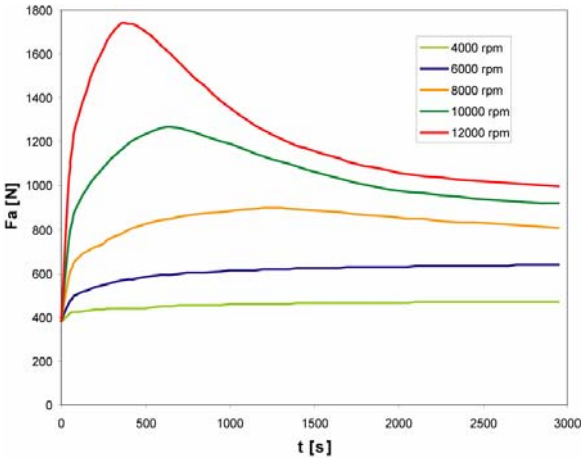

Fig. 22: Preload vs. time, various speeds

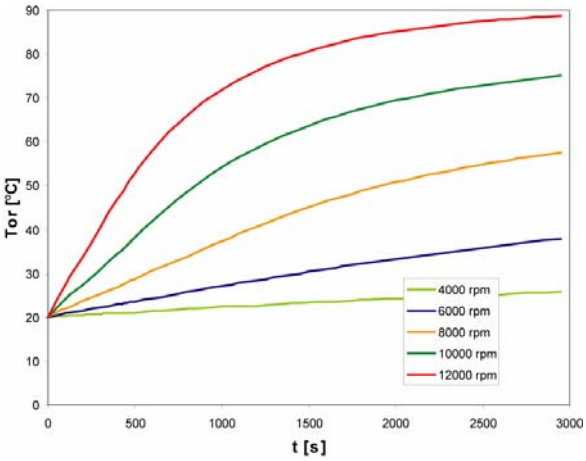

Fig. 23: Outer ring temperature vs. time

The interpretation of such behaviour is described in (Spiewak & Nickel, 2000). First, the temperature of the rolling elements rises rapidly since they receive the largest portion of the heat and their thermal capacity is the smallest, Fig. 25. Preload increases quickly as the rolling elements and the inner ring expand while the size of the outer ring remains almost unaffected, since its thermal capacity is large and the housing acts as a heat sink. The rising preload increases the generated heat, so further expansion of the rolling elements occurs. As the temperature of the outer ring gradually increases, the preload levels off and drops to a new steady state value.

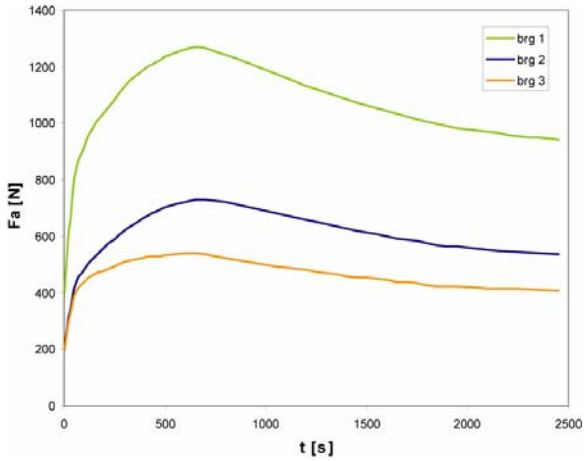

Fig. 24: Preload distribution at 10 000 rpm

Depending upon the dynamics of these changes, the bearings recover without any immediate damage, Fig. 26, or a seizure occurs.

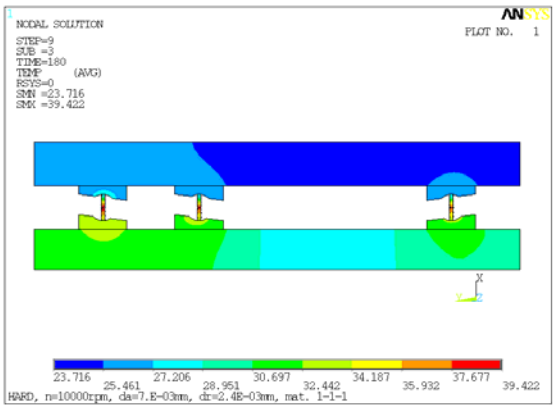

Fig. 25: Temperatures after start

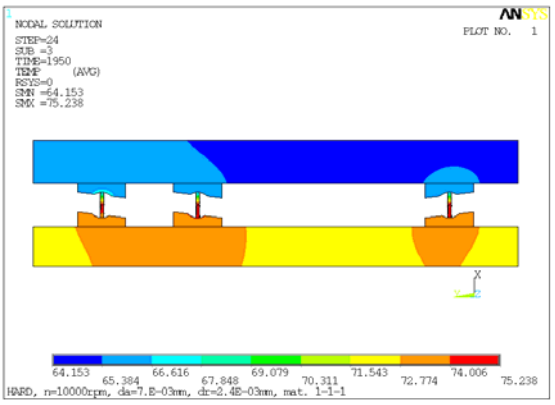

Fig. 26: Temperatures at steady stat

8. Experimental set-up

In high speed bearing systems the operating conditions e.g. contact forces, angles, Hertzian pressure are mostly unidentified. For the purpose of the model validation, an experimental spindle has been designed. It is ready for various bearing configurations, both position and constant preload. It is cheap, comprehensive and equipped with sensors of temperatures and preload. A draft of an instrumented test spindle is shown in Fig. 27. It represents a real triplex set of grease-lubricated bearings SKF 7010 CD.

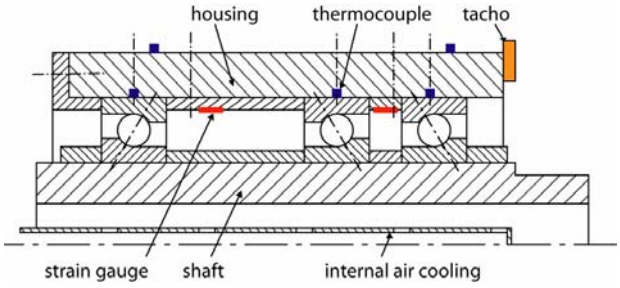

Fig. 27: Test spindle assembly

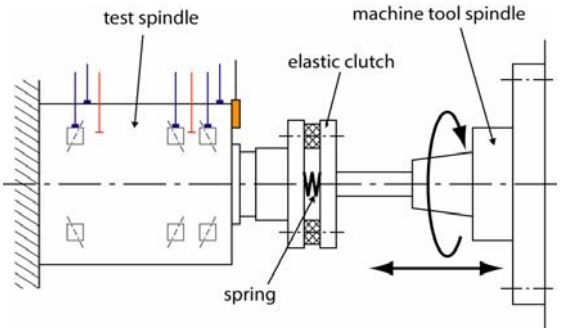

Fig. 28: Drive mechanism

In order to measure axial preloading force during rotation, two stationary housing spacers are equipped with strain gauges. To notice possible misalignment, strain is measured at three positions along the perimeter of each spacer. Thermally compensated strain gauges are used to observe only the deformation caused by loading.

The experimental bearing set is driven externally with a real motorized machine tool spindle connected with a coaxial claw clutch, as shown in Fig. 28. The clutch is equipped with an axial spring to introduce known external axial force (if wanted) to the bearing set by feed of the driving spindle towards the set.

9. Planned experimental investigations

Experiments on the test spindle are focused on particular problems. All measurements are comparable with results of the appropriately adjusted theoretical model described above:

- coast tests, to determine heat generation in bearings
- constant and variable speed tests, to measure temperatures and preload during run
- external force tests, to measure load distribution in the set and changes in thermal stability
- effect of cooling or warming, to compare thermal stability with various coolant air flow or warming tapes on the housing
- effect of initial preload, to investigate behaviour with various initial fits
- bearing configuration tests, to observe the effect of bearing distance by shortening spacers

10. Conclusion

A comprehensive method for prediction of thermo-mechanical behaviour of spindle bearings has been proposed and experimental work is in progress. The 'open source' character of the model allows any additional subroutine to be introduced if it shows up as important during experiments. General methodology of the model could be used as a 'heart' of models of regular motorized spindles. Although validation has not been carried out yet, results of the theoretical model are in proportional agreement with expectations and general experience. It makes it possible to virtually compare various speed conditions, bearing configurations and cooling conditions with thermal stability and high performance considered as the objective.

11. Acknowledgements

This research has been supported by the 1L 6840770003 grant of the Ministry of Education of the Czech Republic. Also thanks to SKF for material support.

12. References

Bossmanns, B., Tu, J.F. (1999) *A thermal model for high-speed motorized spindles*, International Journal of Machine Tools and Manufacture, 39 (9), pp. 13454-1366.

Bossmanns, B., Tu, J.F. (2001) *A power flow model for high speed motorized spindles-heat generation characterization*, Transactions of the ASME, Journal of Manufacturing Science and Engineering, Transactions of the ASME 123 (3), pp. 494-505.

Harris, T.A. (1991) *Rolling bearing analysis*, 3. ed., John Wiley and sons, New York.

Li, H., Shin, Y.C. (2004) *Integrated Dynamic Thermo-Mechanical Modeling of High Speed Spindles Part 1-2*, Journal of Manufacturing Science and Engineering, Transactions of the ASME, 126 (3), pp. 148-168.

Li, H., Shin, Y.C. (1997) *Dynamics of Machine Tool Spindle/Bearing Systems Under Thermal Growth*, Journal of Tribology, Transactions of the ASME, 119, pp. 875-882.

Nakajima, K. (1995) *Thermal contact resistance between balls and rings of a bearing under axial, radial and combined loads*, Journal of Thermophysics and Heat Transfer 9 (1), pp. 88-95.

Spiewak, S.A., Nickel, T. (2001) *Vibration based preload estimation in machine tool spindles*, International Journal of Machine Tools and Manufacture, 41 (4), pp. 567-588.

Stein, J.L., Tu, J.F. (1994) *A state-space for monitoring Thermally-induced preload in anti-friction spindle bearings of high-speed machine tools*, Journal of Dynamic Systems, Measurement and Control, Transactions of the ASME 116 (3), pp. 372-386.